Journal of Zhejiang University-SCIENCE A (Applied Physics & Engineering) 2025 26(4):339-358
www.jzus.zju.edu.cn; www.springer.com/journal/11582
E-mail: jzus_a@zju.edu.cn

Research Article

https://doi.org/10.1631/jzus.A2400359

Thermocline performance in a molten salt thermocline energy storage tank with annular-arranged and cross-arranged diffusers

Zheming TONG[1,2]✉, Haidan WANG[1,2], Shuiguang TONG[1,2], Qi YANG[1,2], Taotao NIE[3]

[1]*State Key Laboratory of Fluid Power and Mechatronic Systems, Zhejiang University, Hangzhou 310058, China*
[2]*School of Mechanical Engineering, Zhejiang University, Hangzhou 310058, China*
[3]*Xizi Clean Energy Equipment Manufacturing Co., Ltd., Hangzhou 310021, China*

Abstract: The thermocline energy storage tank (TEST) serves as a crucial component in thermal energy storage systems, utilizing the working fluid that enters through a diffuser to store and harness energy. However, the conventional double-plate radial diffuser is ill-suited for a single-medium TEST's full tank storage due to its unidirectional fluid inflow. There has been a notable lack of optimization analysis of diffusers. Two innovative tubular diffuser designs with reduced cross-sectional areas have been introduced: the annular-arranged diffuser (AAD) and the cross-arranged diffuser (CAD). To elucidate the impact of diffuser designs on energy storage efficiency, a 3D transient computational fluid dynamics (CFD) model was established to simulate a thermocline formation under two diffuser types. The model was validated against experimental data. Results showed that the thermocline of AAD was 11.39% thinner than that of a traditional double-plate diffuser. In the process of charging and discharging, the time-varying thermocline and factors influencing thermocline thickness were analyzed. Results indicate that in the mixed dominant region, increased turbulent kinetic energy correlates with reduced thermocline thickness. Notably, the AAD's stable thermocline was 4.23% and 5.41% thinner than the CAD's during charging and discharging, respectively, making the AAD preferable for engineering applications. The effects of tube diameter and orifice opening angle on temperature stratification performance were also examined. The findings suggest that an inclined impact jet and large-diameter tubes are more conducive to temperature stratification. Moreover, an orifice diameter optimization method was developed, which can decrease the thermocline by 6.78%.

Key words: Molten salt; Thermocline; Computational fluid dynamics (CFD); Diffuser; Thermal energy storage

1 Introduction

Modern society's increasing reliance on renewable energy and the construction of new power systems has necessitated the development of efficient energy storage technologies. Molten salt, due to its high heat capacity, high energy storage density, and safety, serves as an ideal medium for thermal energy storage systems (Hua et al., 2022; Prieto et al., 2024). A thermocline energy storage (TES) system can be integrated with cogeneration, turbine cycles, and thermal power generation systems to enhance energy use efficiency and flexible transformation (Tong et al., 2022; Kosman et al., 2023; Che et al., 2024; Zhang et al., 2024). Key components within the TES system include the molten salt storage tank, electric heater, and heat exchanger, with the molten salt storage tank accounting for over 40% of the total cost. While the performance and optimization of other energy storage devices have been extensively researched (Mahmoudinezhad et al., 2023; Tong et al., 2023), improving the energy storage efficiency of molten salt storage tanks is paramount.

A thermocline energy storage tank (TEST) is a device that capitalizes on the density differential between cold and hot fluids to create upper and lower layers for energy storage. The cost of a TEST is about 33% lower than that of an equally sized two-tank storage system (Angelini et al., 2014). However, there is inevitable heat loss due to the formation of a thermocline when the cold and hot fluids come into contact. Consequently, recent research in energy storage has

✉ Zheming TONG, tzm@zju.edu.cn
Zheming TONG, https://orcid.org/0000-0003-1129-7439

Received July 19, 2024; Revision accepted Aug. 12, 2024;
Crosschecked Mar. 28, 2025

focused on how to reduce both the thickness of the thermocline and the associated heat loss in TESTs.

The structural parameters and operating conditions of TESTs, especially the type and configuration of the inlet diffuser, have a decisive effect on the thermocline. Scholars have carried out in-depth research on this aspect. A single-medium TEST has a better thermal stratification effect than a packed-bed TEST and multi-medium TEST (ElSihy et al., 2021), while the thermocline is more easily destroyed by an inlet jet. Therefore, it is necessary to study and optimize the diffuser in a single-medium tank. The diffusers in a TEST can be divided into three types according to the flow distribution mode, namely multi-branch flow, inversed flux, and radical flux (Lou et al., 2021). A perforated plate designed for multi-branch flow is generally used in a packed-bed TEST for supporting the solid filler. For a multi-branch flow diffuser, Parida et al. (2022) proposed a hemispherical diffuser and examined the thermal stratifications of the TEST using an ideal stratification index (ISI). Computational fluid dynamics (CFD) and experimental results showed that compared with a diffuser-free inlet, flat plate solid diffuser, and coaxial ring diffuser, the proposed hemispherical diffuser suppressed the mixing of cold and hot fluids. A 2D laminar flow model was used in that study, which has limitations in the simulation of the turbulent structure of fluid near the diffuser. Afrin et al. (2014) proposed a pipe flow distributor for a single-medium molten salt TEST. They investigated the effects of the pipe arrangement and hole position in the distributor on flow and heat transfer in the TEST. They found that the viscous resistance significantly affects the flow exiting through the distributors. Gajbhiye et al. (2022) conducted an experimental study on a single media TEST and showed that a central flow distributor could reduce the thermocline thickness by 50%–60% compared to a TEST without a distributor. Joshi et al. (2021) investigated the effects of the permeability and porosity of the distributor wall on the performance of a porous flow distributor. A thermocline fraction of 13%, the lowest published value, was achieved using a TEST equipped with a porous flow distributor. A shower-type inlet is a medium distributor commonly used in small single-medium TESTs. Li et al. (2014) compared the influences of a slotting-type inlet and shower-type inlet on thermal delamination performance in a water TEST. They concluded that the shower-type inlet could enhance the turbulent action in the TEST and destroy the thermal stratification, and the slotting type is more suitable for solar water heating systems. Chandra and Matuska (2020) studied the performance of a TEST under different working conditions by CFD simulation and experimental analysis, taking the temperature difference, flow rate, and diffuser type as evaluated parameters. Proper selection of the inlet diffuser can greatly optimize the thermal stratification. It is very important to select the right diffuser according to different import and export conditions. A slotted-type inlet can maintain the thermal stratification in the tank well under the conditions of a turbulent inflow and low temperature difference. Kaloudis et al. (2016) numerically studied the gravity current propagation and interaction with solid walls in a TEST and analyzed the influence of flow patterns on mixing during discharging. A nonequal-diameter radial diffuser was proposed by Deng et al. (2021). In addition to studying the effect of structural parameters on diffuser performance, they presented a manual initialization method to shorten the simulation time, which can improve the computational efficiency by about 28.8%. Lou et al. (2020) carried out an optimization analysis of an orifice baffle diffuser in a large single-medium TEST. By modifying the orifice spacing, the evolution of the temperature profiles can be optimized, and the mixing of hot and cold fluids can be suppressed. An innovative TEST equipped with two flat-coil heat exchangers and an internal vertical channel was designed by Cagnoli et al. (2023). They established a CFD model to simulate the buoyancy-driven charging and discharging transients in the system and found that the newly designed structure had higher thermal efficiency than a traditional TEST. Weiss et al. (2021) compared the variation characteristics of thermocline thickness under a simplified 2D diffuser model in three cases: idealized diffuser, and diffusers with and without a flat plate. They conducted a sensitivity analysis on the design parameters of the diffuser to provide optimization guidance. In addition, they suggested that the number and spatial distribution of multi-entry diffusers should be further optimized. Xu et al. (2023) simulated the charging process of a TEST with a plate-type diffuser under the condition of time-varying inlet parameters. They analyzed the exergic efficiency and entropy production rate during the process and the results showed that the thermocline stability is destroyed as the inlet

temperature difference increases. Using a numerical simulation method, Huang and Chen (2016) verified the positive effect of adding thin compartmental plates near the internal walls to avoid heat leakage and determined the best position and size of the plates. By applying this structure, the adiabatic effect of the wall surface of a TEST can be effectively improved.

Experimental studies on different aspects of TESTs have also been carried out. Pacheco et al. (2002) conducted experimental research on the thermocline properties of a small molten salt TEST and recorded the temperature characteristics of molten salt during the discharging process. Nallusamy et al. (2006) obtained experimental estimates of the performance of a packed bed with phase change material (PCM) TEST under different inlet conditions. They concluded that mass flow is a key factor affecting the heat storage efficiency. Cheralathan et al. (2006) investigated the transient behavior of PCMs in thermal energy storage systems and designed experiments to validate the developed simulation program. The results showed that porosity is an important factor affecting PCM energy storage. Shi et al. (2021) experimentally studied the solidification and migration behavior of molten salt in a TEST under different leakage conditions. An experiment aiming to measure the heat transfer enhancement effect of gas injection on a TEST was designed by Che et al. (2024). The relationship between the heat transfer coefficient and the gas injection rate was investigated. The results showed that the gas injection method could improve the performance of a single-tank system, but would cause energy loss. Lou et al. (2023a, 2023b) designed a single-medium TEST with ring-opening plate distributors (ROPDs). They obtained the transient flow field and temperature field characteristics of a TEST through CFD simulation, and designed experiments to observe the charging and discharging process with different ROPD designs. The results showed that an optimized ROPD structure can effectively alleviate the strong inertia force of the hot jet and significantly improve the overall performance of the thermocline. They observed the evolution process of the impact jet in a TEST system by combining the particle image velocimetry (PIV) method with CFD simulation, and designed ROPDs to optimize the overall performance of the TEST. Yin et al. (2017) designed an experiment to validate a simulation model based on 2D local thermal equilibrium theory in a porous packed-bed TEST charging process. Neglect of the inlet effect in the simulation model caused deviation between the results of the experiment and simulation. They also found that the heat storage efficiency of the porous packed-bed TEST was lower than that of a pure molten salt TEST. Cascetta et al. (2016) observed the heat energy storage behavior of a packed-bed TEST through experiments and established a CFD analysis model based on non-equilibrium heat transfer of two-phase flow. When the model adopted was consistent with the experimental inlet temperature setting, the experimental and simulation data had high coincidence. Keilany et al. (2020) experimentally compared the performances of a packed-bed TEST filled with solid waste Cofalit® and alumina spheres. The thermocline thickness and the process efficiency of the Cofalit® were 19.6% thinner and 6.1% higher than those of the alumina spheres, respectively. The vitrified waste filling material provides the possibility for sustainable development of environmentally sound energy.

In terms of numerical characterization methods for TEST systems, Votyakov and Bonanos (2015) summarized the empirical formula of thermocline thickness using an algebraic method, and expressed the thermocline thickness by the dimensionless Peclet number (*Pe*) and Biot number (*Bi*). Pizzolato et al. (2015) used a numerical method to fit the thermocline characterization function in a TEST system according to CFD simulation results. The reduced model had good universality and was suitable for system-level annual simulations. Manu et al. (2015) simulated the Rayleigh-Taylor instability in a TEST system under different inlet temperature perturbations and studied the flow coherent structure during thermocline mixing. A thermocline breakdown was observed at high Atwood number (*A*). Hosseinnia et al. (2021) proposed a new criterion for quantifying thermocline thickness (TLT) based on 1 K below maximum temperature (T_{max}) and 1 K above minimum temperature (T_{min}) inside a TEST. The minimum defined TLT is proportional to the square root of the dimensionless storage time divided by the Peclet number. In addition, the TLT in the non-ideal state with heat loss and turbulent mixing effects was simulated. Khurana et al. (2024) established a reduction-order realistic stratification (RS) model to predict the TLT of a TEST. The model had high accuracy and reduced the calculation time by 80% compared with the CFD method.

Previous research has usually simplified the inlet and outlet in a TEST to an ideal diffuser, characterized by an inlet with uniform velocity and temperature. However, there are always inlet turbulence effects in a real TEST, which will affect the temperature distribution and even the operating stability of the TEST system. Moreover, a traditional double-plate radial diffuser has a high cross-sectional area ratio, and the fluid inflow can be designed in only a single direction, which is not suitable for the full tank storage of molten salt. A tubular diffuser has a small cross-sectional area ratio. With a reasonable impact jet angle and orifice size design, the disturbance of the jet to the fluid can be reduced and thermocline viscous fingering can be avoided. Therefore, in this study, annular-arranged and cross-arranged tubular diffusers were designed, and a CFD model based on a realistic TEST was devised to explore the influence of different diffusers on the temperature field. The charging and discharging processes of the two kinds of TEST diffusers were simulated, and the uniformity of circumferential temperature distribution and the variation of thermocline under the two designs were compared. Concurrently, the influence of tube diameter and orifice opening angle on temperature stratification was investigated. An optimization method to reduce the thermocline by adjusting the orifice opening size was also developed.

2 Methods

2.1 Geometrical model and parameters definition

A schematic diagram of the TEST is shown in Fig. 1a. The TEST simultaneously stores hot and cold molten salts in one tank. The difference in density between the hot and cold molten salts forms a natural stratification phenomenon. Hot and cold molten salts enter the tank through the diffusers arranged at the top and the bottom, respectively. There is a large temperature gradient between the high-temperature and low-temperature molten salts, that is, the thermocline. The smaller the thickness of the thermocline, the smaller the heat loss and the higher the heat storage efficiency of the TEST.

In this study, two different diffuser arrangements in the TEST were designed and simulated: a cross-arranged diffuser (CAD) and an annular-arranged diffuser (AAD). A geometric model of the tank is shown in Fig. 1b, and geometric diagrams of the CAD and

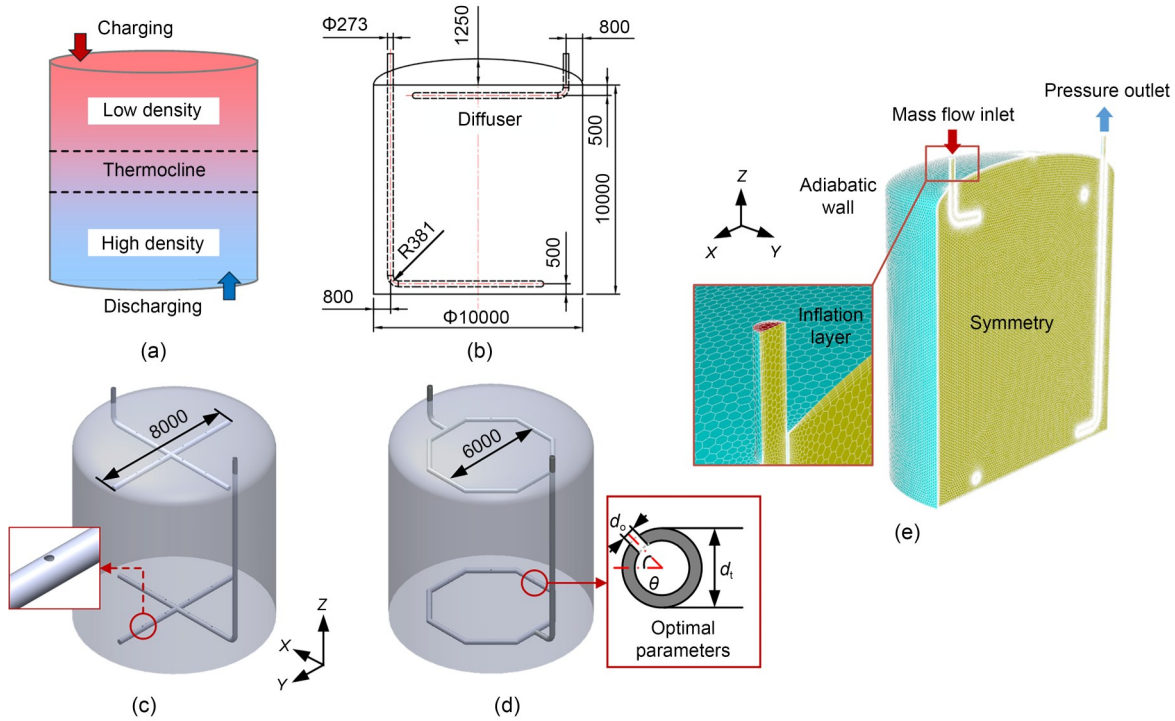

Fig. 1 (a) TEST working principle; (b) dimensions of the TEST tank; (c) cross diffuser arrangement; (d) annular diffuser arrangement; (e) meshing and boundary condition settings (unit: mm)

AAD are shown in Figs. 1c and 1d, respectively. The thickness of the diffuser tube was 10 mm, and eight orifices were evenly distributed along the horizontal tube. The design optimization of the diffuser mainly involves adjustments to the tube diameter d_t, orifice opening angle θ, and orifice diameter d_o.

After determining a suitable design for the arrangement, the effects of tube diameter and orifice angle on thermal stratification and flow patterns were analyzed. The different case settings are shown in Table 1.

Table 1 Case settings

Case	Arrangement	Tube diameter, d_t (mm)	Orifice opening angle, θ (°)
1	CAD	273	90
2	AAD	273	90
3	AAD	273	60
4	AAD	273	45
5	AAD	273	0
6	AAD	233	45
7	AAD	313	45
8	AAD (optimal orifice diameter)	313	45

The low and high molten salt temperatures were 553 and 773 K, respectively. The hot fluid flows through the up diffuser during the charging process, and the cold fluid flows through the bottom diffuser during the discharging process. The molten salt inlet flow rate was 159.8 t/h, and the pressure was 1 MPa, according to the actual working conditions.

The calculation domain was established by volume extraction of the TEST model. Due to its axisymmetric characteristics, half of the model was taken for calculation, the Y=0 plane was set as the symmetric boundary, and the wall was simplified as the adiabatic wall. Fluent meshing was used and inflation layers were added to the wall (Fig. 1e).

Molten salt with a specific composition of 60% $NaNO_3$ and 40% KNO_3 was selected as the working fluid in this study. The freezing and pyrolysis temperatures of the molten salt were 513 and 838 K, respectively. The thermophysical properties are shown in Table 2.

Since the region with the largest temperature gradient variation in the thermocline is concentrated in the middle 70% of the thickness range, T^*=0.15–0.85 was taken, corresponding to the actual temperature T of 586–740 K, where T^* is defined as:

Table 2 Properties of the molten salt

Property	Description
Density, ρ (kg/m^3)	$2090-0.636T$
Specific heat capacity, c_p (J/(kg·°C))	$1443+0.172T$
Viscosity, μ (Pa·s)	$2.2714\times10^{-2}-1.2\times10^{-4}T+2.281\times10^{-7}T^2-1.474\times10^{-10}T^3$
Thermal conductivity, λ (W/(m·K))	$0.443+0.00017T$

T is the temperature (K)

$$T^* = \frac{T - T_{\min}}{T_{\max} - T_{\min}}. \tag{1}$$

The dimensionless thickness T_K^* is defined as:

$$T_K^* = h_{0.85}^* - h_{0.15}^*, \tag{2}$$

where $h_{0.85}^*$ and $h_{0.15}^*$ are the dimensionless heights of the fluid at temperatures of T^*=0.85 and T^*=0.15, respectively.

The dimensionless height h^* is defined as:

$$h^* = \frac{h}{H}, \tag{3}$$

where h is the height and H is the total height of the fluid zone. Because of the vaulted top of the TEST, the average height H was taken as 10.84 m in this study.

The dimensionless volume of the thermocline V_{TK}^* is defined as:

$$V_{TK}^* = \frac{V_{TK}}{V_{\text{tank}}}, \tag{4}$$

where V_{TK} is the volume of the thermocline and V_{tank} is the volume of TEST. The value of V_{tank} was 850.89 m^3 in this study. V_{TK} can be obtained by integrating the thermocline volume.

The variation coefficient C_V was used to describe the uniformity of temperature distribution:

$$C_V = \frac{T_{\text{rms}}}{T_{\text{avg}}} \times 100\%, \tag{5}$$

$$T_{\text{rms}} = \sqrt{\frac{\sum_{i=1}^{N}(T_i - T_{\text{avg}})^2}{N}}, \tag{6}$$

where T_{avg} is the average temperature, T_i is the temperature of the ith sampling point, and N is the number of sampling points.

2.2 Flow field solving method

The simulations were performed using ANSYS Fluent 19.2, and the Navier-Stokes and energy equations were used to solve the transit-state fluid and thermal fields. The mass continuity equation, momentum continuity equation, and energy continuity equation of the fluid were as follows:

$$\frac{1}{r}\left[\frac{\partial(\rho ru)}{\partial x}+\frac{\partial(\rho rv)}{\partial r}\right]=0, \tag{7}$$

$$\frac{1}{r}\left\{\frac{\partial(\rho ru)}{\partial t}+\frac{\partial[(\rho rv)u]}{\partial r}-u\left[\frac{\partial(\rho ru)}{\partial x}+\frac{\partial(\rho ru)}{\partial r}\right]\right\}=-\frac{\partial P}{\partial x}+\frac{1}{r}\left[\frac{\partial}{\partial x}\left(ur\frac{\partial u}{\partial x}\right)+\frac{\partial}{\partial r}\left(ur\frac{\partial u}{\partial r}\right)\right]+\rho g\beta(T-T_0), \tag{8}$$

$$\frac{1}{r}\left\{\frac{\partial(\rho rT)}{\partial t}+\frac{\partial[(\rho rv)T]}{\partial x}+T\left[\frac{\partial(\rho ru)}{\partial x}+\frac{\partial(\rho ru)}{\partial r}\right]\right\}=\frac{1}{r}\left[\frac{\partial}{\partial x}\left(\frac{k}{c_p}r\frac{\partial u}{\partial x}\right)+\frac{\partial}{\partial r}\left(\frac{k}{c_p}r\frac{\partial u}{\partial r}\right)\right], \tag{9}$$

where t, r, x, u, and v represent the time, radial coordinate, axial coordinate, axial velocity, and radial velocity, respectively. g is the gravitational acceleration, P is the pressure, β is the coefficient of thermal expansion, T_0 is the reference temperature, and k is the thermal conductivity.

Due to the XY plane symmetry of the TEST, half of the symmetrical geometry was selected as the calculation domain to reduce the number of grids and improve the calculation efficiency. In the actual working process, the tank was composed of multi-layer insulation materials, so the wall was set as a non-slip adiabatic boundary. The velocity inlet and pressure outlet were set as the boundary conditions. Molten salt is an incompressible fluid, regardless of the viscous dissipation effect inside the fluid, and its temperature variation characteristic is realized by user-defined functions.

A transient solver was used to calculate the constant change of molten salt temperature. The energy equation was used for solving the temperature change of molten salt. Considering the influence of gravity on the flow field and temperature field, the gravitational acceleration was g=9.81 m/s^2. To calculate the turbulence effect, the standard $k-\varepsilon$ turbulence model was used for simulation.

$$\frac{\partial}{\partial t}(\rho k)+\frac{\partial}{\partial x_i}(\rho k u_i)=\frac{\partial}{\partial x_j}\left[\left(\mu+\frac{\mu_t}{\sigma_k}\right)\frac{\partial k}{\partial x_j}\right]+\frac{1}{2}p_{ij}-\rho\varepsilon, \tag{10}$$

where ε is the turbulent dissipation rate, μ_t is the turbulent viscosity, σ_k is the turbulent Prandtl number, and p_{ij} is the rate of production of turbulent kinetic energy.

A double precision solver was used to solve the problem, and the discrete scheme was adopted as the second-order upwind. The SIMPLE (semi-implicit method for pressure-linked equations) algorithm was used to solve the pressure–velocity coupling equation.

2.3 Optimization method

The flow in the diffuser tube was not uniform and the flow rate and velocity of the impact jet through each orifice were not consistent, which caused a mixing of the cold and hot fluids. An algorithm for optimizing the diffuser orifice size was developed to keep the impact of the jet flowing from different orifices consistent and minimize the impact of the impact jet on the thermocline. The overall optimization process for the TEST is as follows (Fig. 2).

Firstly, to clarify the arrangement of the diffuser, determine the opening direction of the orifices and select the diameter of the tube. Obtain the velocity and pressure profile in the tube and mass flow rate of each orifice jet outlet under the design.

Number the orifice nearest to the inlet as orifice 1 and number the remaining orifices consecutively clockwise. An iteration is done by calculating the deviation between the flow rate of each orifice (q_i) and the average flow rate ($\bar{q}$) to determine the orifice size. In step j, if q_{j-1} is less than the $\bar{q}$, r_i will be expanded. Else, r_i will be reduced. γ is the adjusting factor.

$$\Delta r_j=r_{i,j}-r_{i,j-1}=\gamma(q_{i,j}-\bar{q}_j). \tag{11}$$

The average flow rate $\bar{q}$ is calculated as follows:

$$\bar{q}=\frac{\sum\rho_i\cdot v_i\cdot\pi r_i^2}{8}. \tag{12}$$

The standard deviation (D_S) of the mass flow rate is monitored in each iteration.

$$D_{S,q_i}=\sqrt{\frac{1}{8}\sum\left(\frac{q_i-\bar{q}}{\bar{q}}\right)^2}. \tag{13}$$

The optimization is considered to be complete when the decline of dimensionless thermocline volume V_{TK}^* is less than 1%.

2.4 Grid and time step independence verification

In this study, grid independence verification was carried out under three grid sizes: 0.8 million (Mesh 1), 1.4 million (Mesh 2), and 1.8 million (Mesh 3). Grid independence was tested by monitoring the average temperature change of the Z=10 m plane in 2 h under the charging process in Case 2. The results showed that when the number of cells reached 1.4 million, the temperature change was less than 0.08%, so Mesh 2 was selected for calculation.

The time step size was set to 5 s according to the Courant number, with 10 iterations in each time step, and the total number of time steps was 2880 for modelling the charging and discharging process in the first 4 h. The time step independence of the Case 2 model was verified. The temperature distribution on the central axis of the storage tank after 3 h was extracted (Fig. 3b). When the time step reduced from 5 s to 3 s, the temperature change was less than 0.16%.

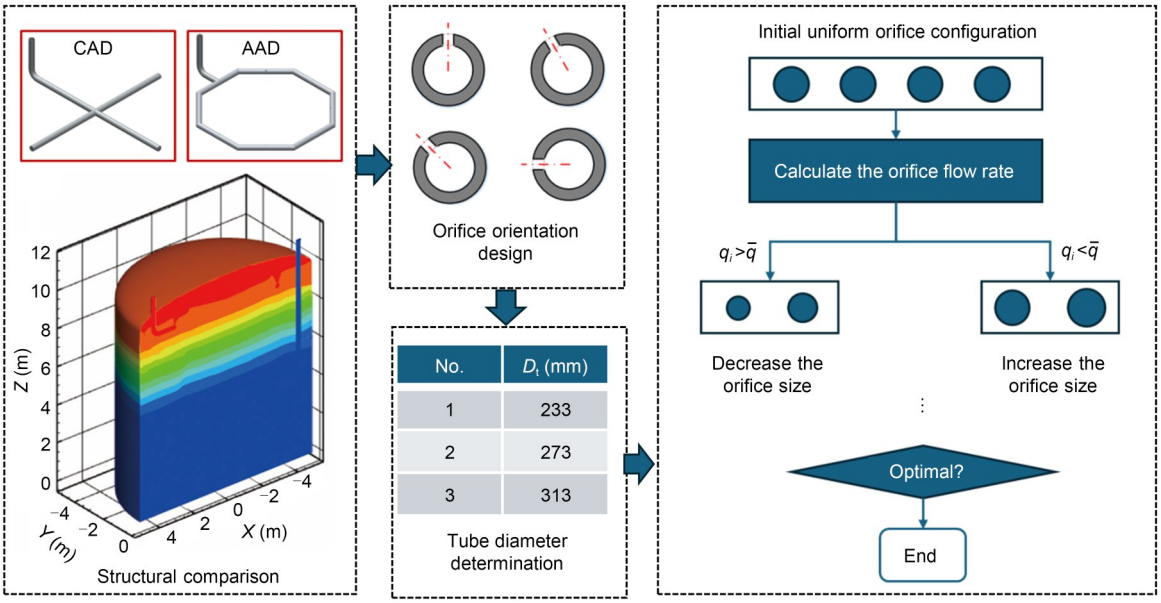

Fig. 2 Optimization method

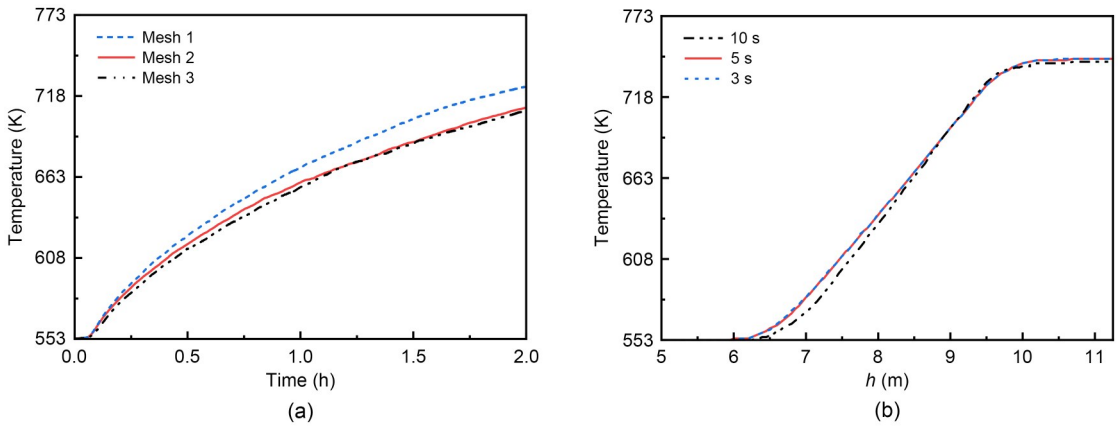

Fig. 3 (a) Grid independence verification; (b) time step independence verification

3 Results and discussion

3.1 Validation of CFD simulation

To ensure the reliability of the simulation method proposed in this study, the simulation results were compared with the experimental data obtained by Lou et al. (2023b) in Fig. 4. The model construction was consistent with the experimental conditions, and water was used as the energy storage fluid. The interior of the tank was extracted as the fluid domain, 1/4 of the overall model was used for simulation, and the boundary condition setting and simulation methods described in Sections 2.1 and 2.2 were used for simulation. During the calculation, temperature change curves of points TC3, TC4, TC5, and TC6 on the central axis were monitored. The positions of the points are described in the reference (Lou et al., 2023b).

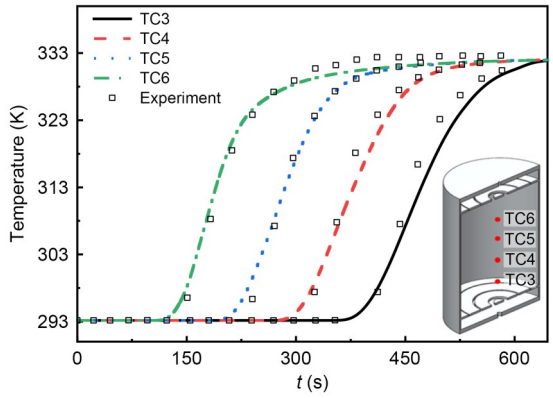

Fig. 4 Comparison of simulation results and experimental data

The simulation results were consistent with the trend of the experimental data, and the maximum error with the referenced simulated data was less than 3%. Therefore, the simulation method proposed in this study can be considered credible.

3.2 Thermocline performance under different arrangements of diffusers

3.2.1 Comparison of classic plate diffuser and the proposed AAD

To evaluate the performance of the proposed tubular diffuser, we compared the temperature delamination characteristics of a classic plate diffuser and the AAD after 4 h. This comparison was represented by the surface mean temperature along the axial direction and the dimensionless thermocline volume V^*_{TK} (Fig. 5). The positioning of the plate diffuser and the tank's dimensions were consistent with those of the AAD shown in Fig. 1d. The diameter of the inlet tube was 273 mm, and the plate diameter was 6000 mm.

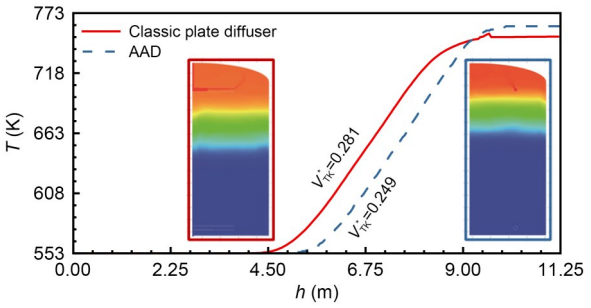

Fig. 5 Temperature delamination characteristics of the TEST with a classic plate diffuser and the AAD in 4 h

A singularity in temperature distribution occurred near the height of 9.5 m in the classic plate diffuser. This phenomenon was attributed to the mixing and stratification of hot and cold fluids within the diffuser during the flow of the hot fluid through the plate. Consequently, the temperature of the fluid near the upper plate is closer to the initial hot fluid temperature. In the planes situated above the plate diffuser, the blending of hot and cold fluids leads to heat loss, resulting in a temperature that is lower than the hot fluid inlet temperature. Compared with conventional plate diffusers, AAD reduced the thermocline volume by 11.39%.

3.2.2 Thermocline performance in the charging process

Fig. 6 illustrates the temperature distribution contours in the TEST over 1–4 h, a period characterized by a mixed dominant stage before the complete formation of the thermocline. Initially, during energy storage, the buoyancy effect due to low density causes the hot fluid to rise spontaneously. This movement induces heat exchange between the cold and hot fluids, leading to energy loss from the hot fluid. The overall temperature field characteristics exhibit minimal differences between the two configurations within the first 1–2 h. However, at 3 h, the top temperature in the CAD arrangement surpasses that of the AAD. By 4 h, the peak temperature of the hot fluid at the top of the TEST nearly equals the inlet temperature.

Temperature sampling along the *Z*-axis was conducted to gather temperature distribution data for the internal line segment from 1–4 h (Fig. 7). The data

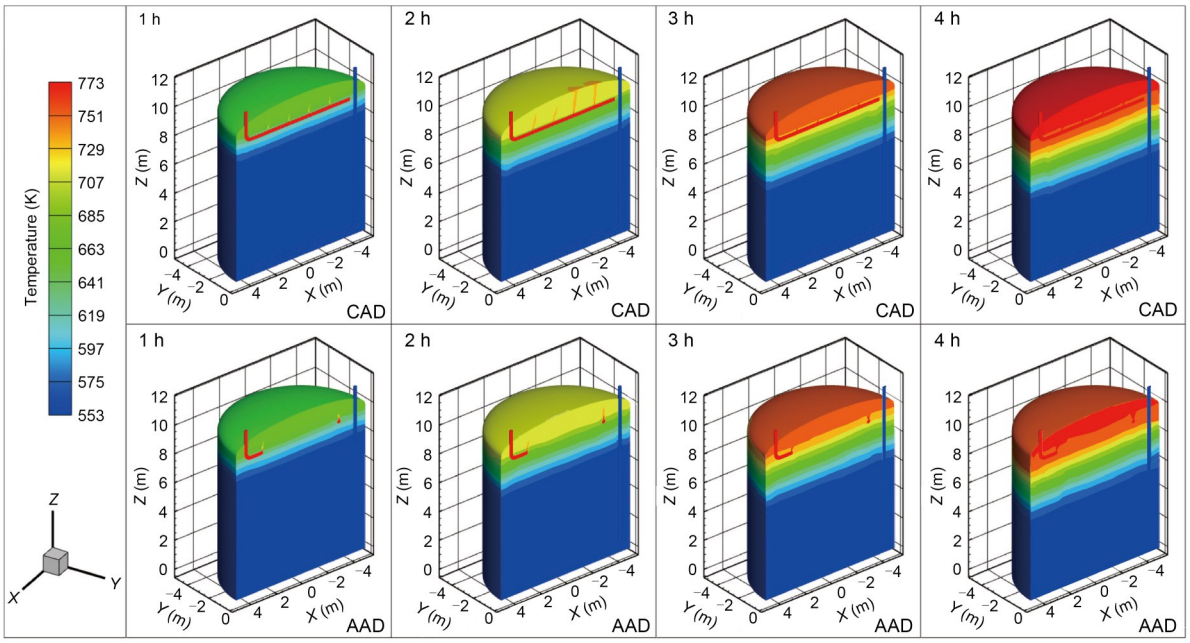

Fig. 6 Temperature field distribution inside the TEST during the charging process

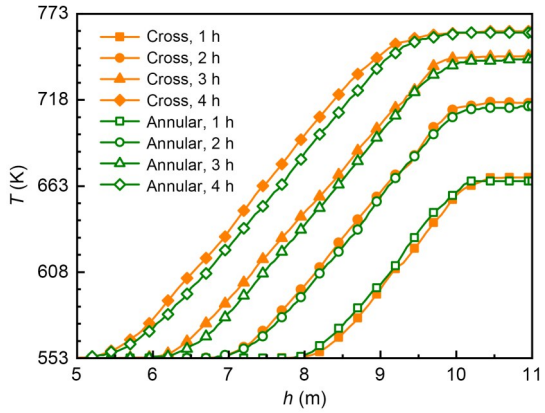

Fig. 7 Temperature curve along the *Z*-axis in the charging process

revealed that there was minimal temperature difference between the two diffusers in the first 2 h. However, in the subsequent 2 h, the temperature curve for AAD becomes steeper, suggesting a smaller thermocline thickness for the AAD. At the same height, the temperature of the CAD exceeded that of the AAD, implying that the CAD mixes hot and cold fluids more effectively. This heat transfer mechanism reduced thermal stratification in the TEST.

The variation in thermocline thickness in the X plane is illustrated in Fig. 8. The tank profile's irregularity caused the thermocline thickness to be inconsistent in the Z direction due to disturbances. During the initial 2 h, the thermocline did not fully form, rendering the dimensionless V_{TK}^{*} inappropriate for representing this period. Consequently, image processing techniques were used to compute the thermocline thickness and the section area percentage. The results are summarized in Table 3. From 1 to 2 h, the thermocline remained underdeveloped, with flow mixing predominating in the TEST phase. Moreover, the thermocline movement in AAD was slower than in CAD, resulting in a smaller thickness. This observation indicates that the stratification of hot and cold fluids is more effective in AAD, leading to reduced thermal energy loss. By 4 h, a stable thermocline was deemed to have formed within the system, with the AAD thermocline being 4.23% thinner than its CAD counterpart.

The diffuser layout plane (Z=9.5 m) was selected to compare temperature contours between the AAD and CAD from 1–4 h in the charging process (Fig. 9). The average temperature of the CAD was higher than that of the AAD. Combined with the analysis of Figs. 7 and 8, we conclude that the heat transfer activity of the CAD was more active in the axial direction, while the turbulent diffusion effect of the AAD was more obvious in the circumferential direction, so the temperature difference of the AAD was more obvious than that of the CAD in the diffuser plane.

The temperature in the diffuser plane was sampled with a sampling step of 0.01 m, and the temperature

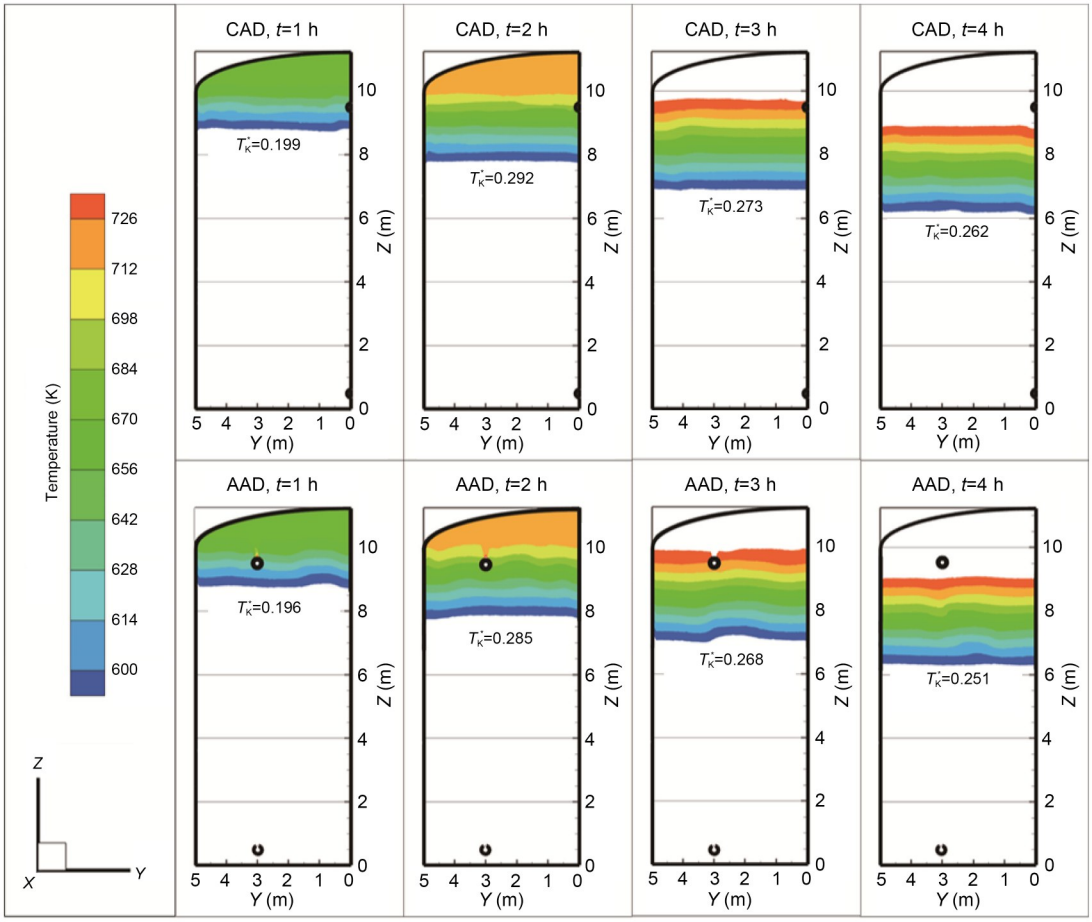

Fig. 8 Thermocline thickness chart in the charging process

Table 3 Thermocline proportion in the charging process

Diffuser	Thermocline proportion (%)			
	t=1 h	t=2 h	t=3 h	t=4 h
CAD	19.49	28.65	26.03	24.84
AAD	19.22	27.97	25.56	23.79

uniformity was quantified by calculating the average temperature T_{avg} and variation coefficient C_V. The results are shown in Fig. 10. The average temperature of the CAD was higher than that of the AAD, while the variation coefficient was lower. This shows that during the mixing-dominated stage, the horizontal heat exchange inside the thermocline formed by CAD is weaker.

Fig. 11 illustrates the surface average turbulent kinetic energy distribution curve for planes above the diffuser. A plane was positioned 0.25 m above the diffuser to calculate the area average of turbulent kinetic energy, thereby measuring the energy dissipation caused by different diffuser arrangements. At the Z=9.50 m plane, the turbulent kinetic energy intensity exceeded that at the plane below the working height of the tank (Z=10.00 m) due to the turbulent flow in the diffuser tube. In the mixed dominant region, the turbulent kinetic energy of the AAD gradually increased with time, while the turbulent kinetic energy intensity of CAD did not exceed 5% in each plane over time. Therefore, we conclude that the enhancement of turbulent kinetic energy contributed to the thinning of the thermocline during the mixing-dominated process.

3.2.3 Thermocline performance in the discharging process

Given the vaulted top and flat bottom of TEST, the discharging process cannot merely be considered as the reverse of charging. Consequently, an analysis of the discharging process flow was conducted.

Fig. 12 shows the contours of the TEST temperature change during 1–4 h of the discharging process. The complete thermocline was formed faster than the

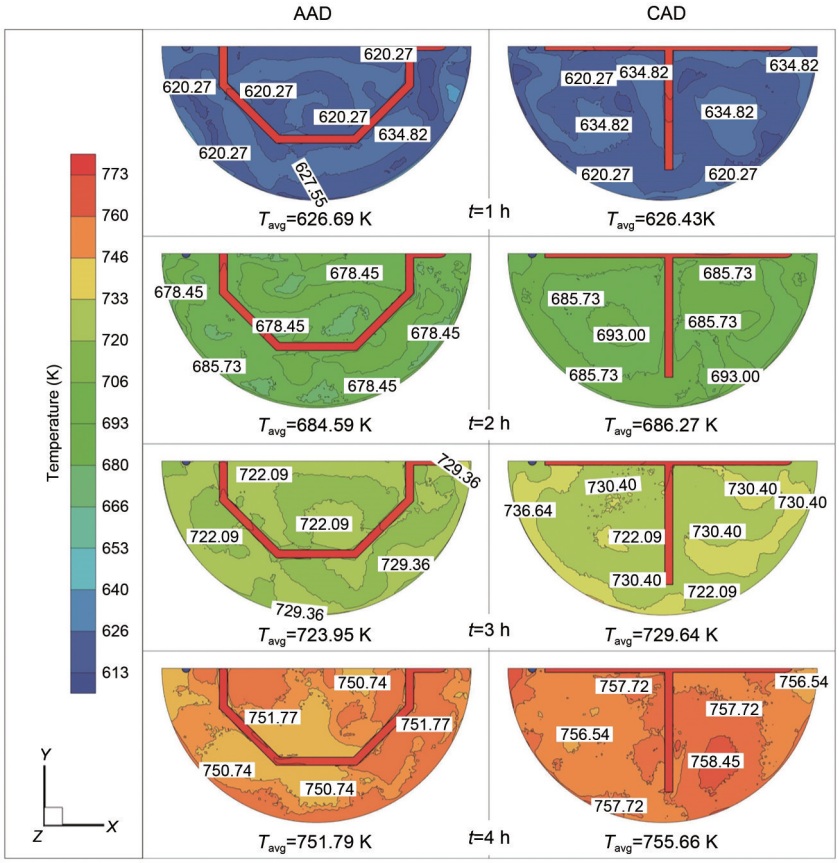

Fig. 9 Temperature contours in the diffuser plane of the AAD and CAD in the charging process

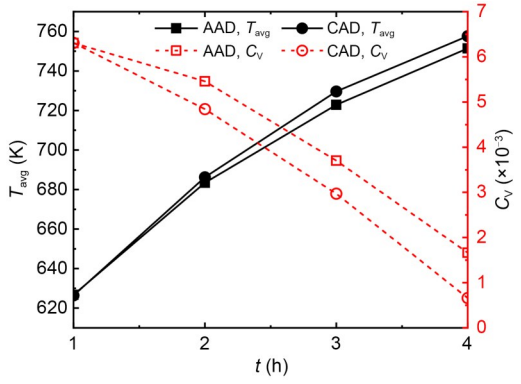

Fig. 10 Average temperature and variation coefficient in the charging process

charging process due to the proximity of the diffuser to the bottom and the shorter time required for the mixing process.

Note that at the diffuser orifice outlet, the cold fluid was first directed upward by the inertial force and then downward due to the density gradient.

Fig. 13 illustrates the temperature change curve along the *Z*-axis during the discharging process. The temperature variations of the AAD and CAD were not significantly different from those of the charging process. This similarity arises due to the equal distance between each diffuser orifice and the bottom surface, leading to faster thermocline formation. Generally, the slope of the curve in the CAD was marginally lower than that in the AAD, and the temperature at the same position and time was slightly lower in the CAD than in the AAD.

The variation in thermocline thickness under discharging conditions is shown in Fig. 14, while Table 4 presents the proportional area of the thermocline. Compared to the heat storage condition, the thermocline thickness during discharging was markedly reduced, particularly at 3 h. This reduction can be attributed to the fact that during heat storage, the hot fluid must flow to the vaulted top, with the center height to the diffuser measuring 1.75 m. Conversely, the distance from the bottom to the diffuser plane was 0.50 m, resulting in a smaller mixing area for the hot and cold fluids, which accelerates the formation of the thermocline. Additionally, it is important to highlight that at *t*=2 h,

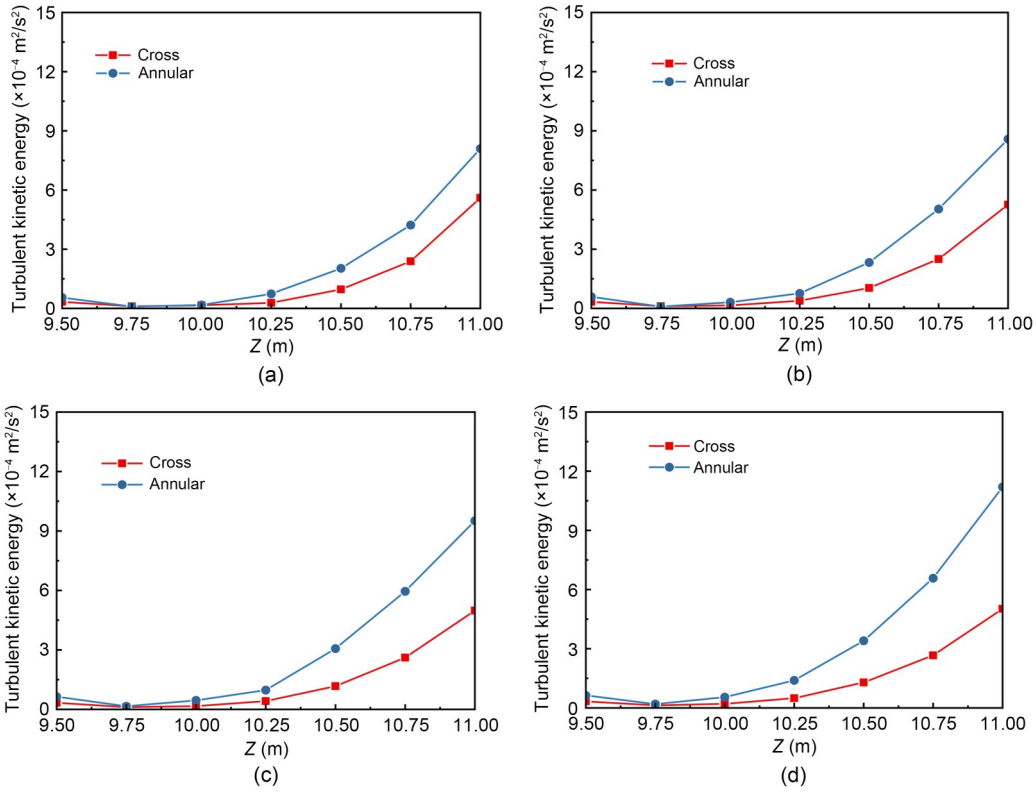

Fig. 11 Turbulent kinetic energy distribution in the charging process: (a) 1 h; (b) 2 h; (c) 3 h; (d) 4 h

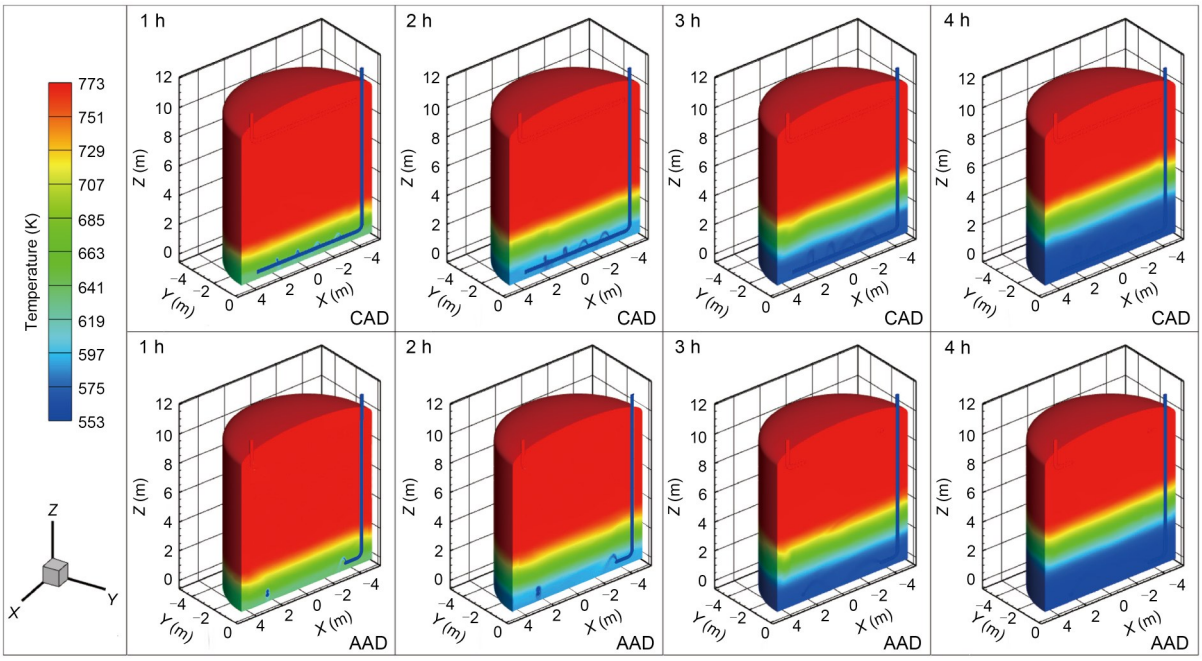

Fig. 12 Temperature field distribution inside the TEST during the discharging process

the bottom temperature of the AAD first fell below the critical value. The thermocline of the AAD was 5.41% thinner than that of the CAD during discharging.

Fig. 15 shows the contours of temperature variation at the plane where the diffuser was located during discharging. It is evident that due to the flat bottom of

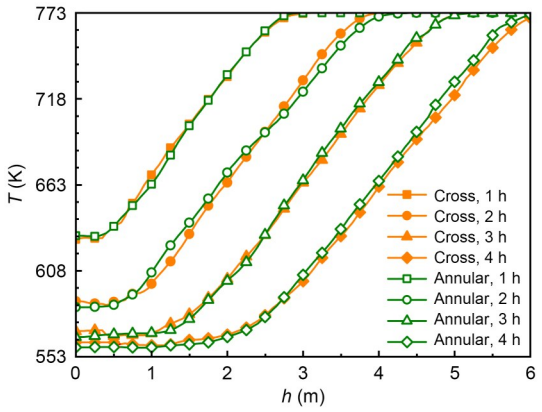

Fig. 13 Temperature curve along the *Z*-axis during the discharging process

the tank, the temperature uniformity was significantly higher than that during the charging process. Additionally, the AAD's plane temperature uniformity was lower and exhibited more intense turbulence.

The quantitative results of temperature uniformity are shown in Fig. 16. In contrast to the charging process, the difference in the diffuser plane temperature variation coefficient caused by the two arrangements is the largest at the beginning, and then decreases. This is because the mixing effect of hot and cold fluids is the strongest at 1 h, and the thermocline gradually forms after 2 h, leaving the diffuser plane.

Below the diffuser plane (Z=0.5 m), surface turbulent kinetic energy was calculated every 0.125 m

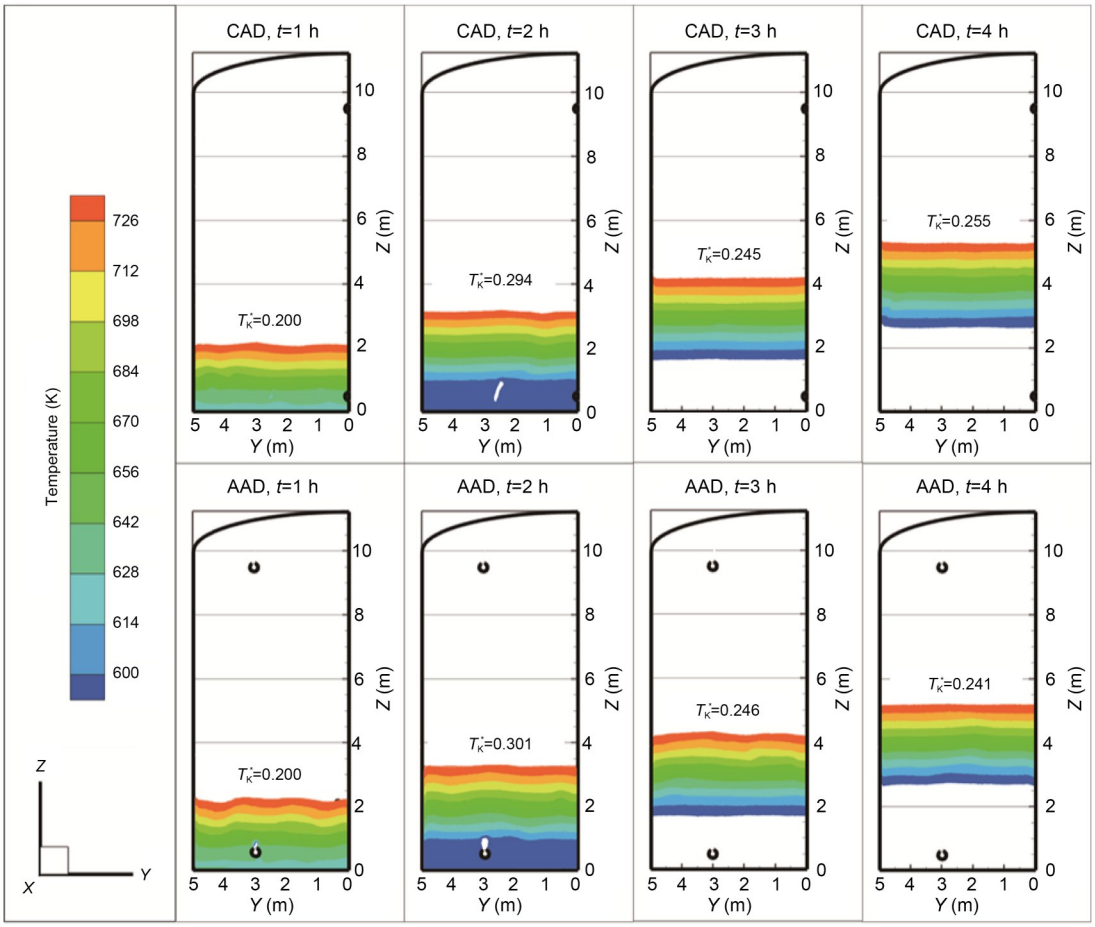

Fig. 14 Thermocline thickness chart during the discharging process

Table 4 Thermocline proportion during the discharging process

Diffuser	Thermocline proportion (%)			
	t=1 h	t=2 h	t=3 h	t=4 h
CAD	18.77	28.12	23.62	24.40
AAD	18.77	28.70	23.62	23.08

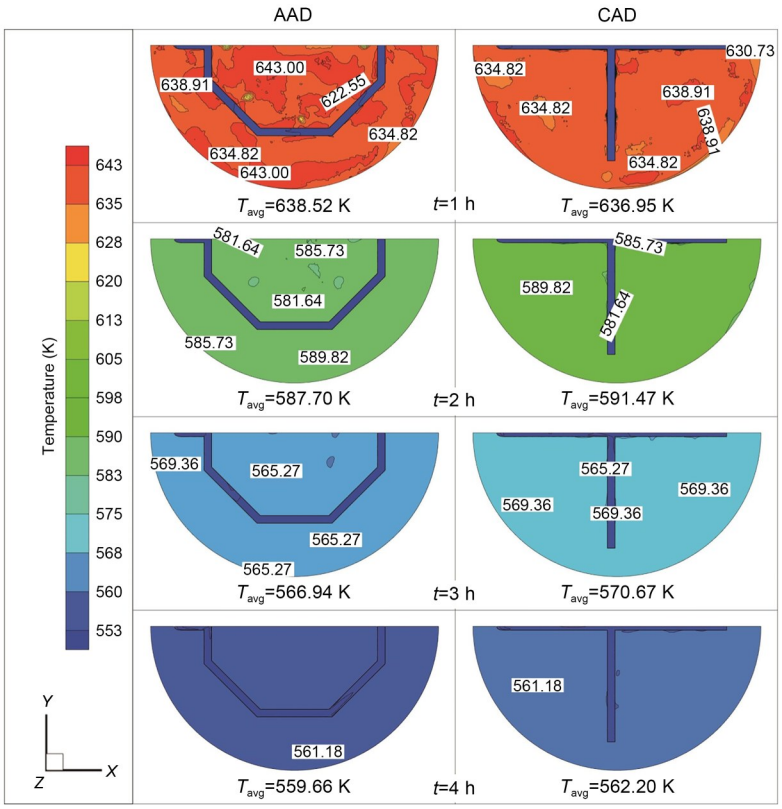

Fig. 15 Temperature contours in the diffuser plane of the AAD and CAD during the discharging process

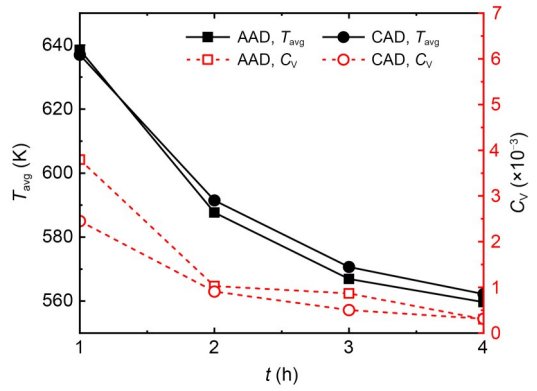

Fig. 16 Temperature contours in the diffuser plane during the discharging process

(Fig. 17). The turbulent kinetic energy of the AAD was always greater than that of the CAD, and the difference between the two was smaller than that in the charging process. Therefore, the difference in temperature uniformity was also smaller than in the charging process. Below the diffuser plane, the turbulent kinetic energy was one order of magnitude higher than above it because the cold fluid flows in and sinks to the bottom under buoyancy.

Because the jet does not interact directly with the wall surface during the discharging process, the variation trend of the CAD and AAD thermoclines under the discharging condition did not differ much from the temperature profile in the tank compared with during the charging process. However, the interaction between the jet and vault will affect the thermal delamination performance of the TEST, so Sections 3.2 and 3.3 discuss the influence only of different structural parameters on thermocline performance under heat storage conditions.

3.3 Influence of orifice orientation on thermal stratification

In the initial stage of charging, the density of the impact jet differs significantly from that of the fluid in the tank. This difference is influenced by buoyancy and results in a strong mixing effect between the cold and hot fluids. Consequently, the jet velocity profile after 1 h of charging was chosen for observation. The velocity contours of the orifice outflow in the X=0 plane are compared in Fig. 18. The vertical opening direction of the orifices allows the outflow to jet upward

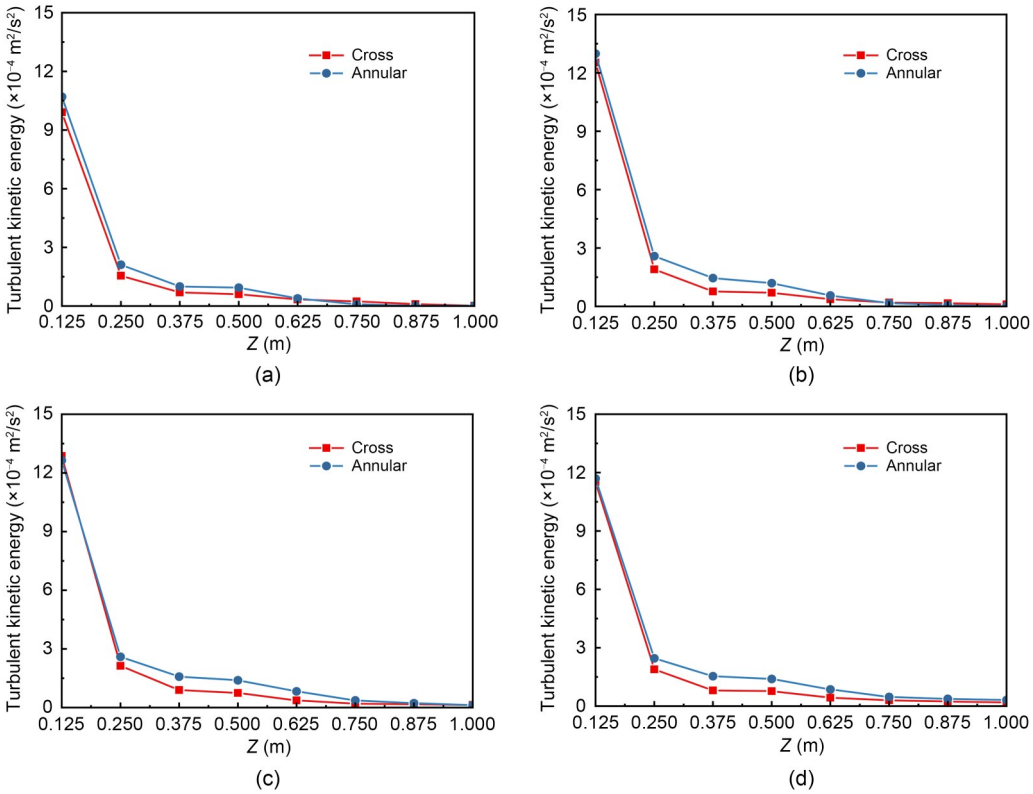

Fig. 17 Turbulent kinetic energy distribution during the discharging process: (a) 1 h; (b) 2 h; (c) 3 h; (d) 4 h

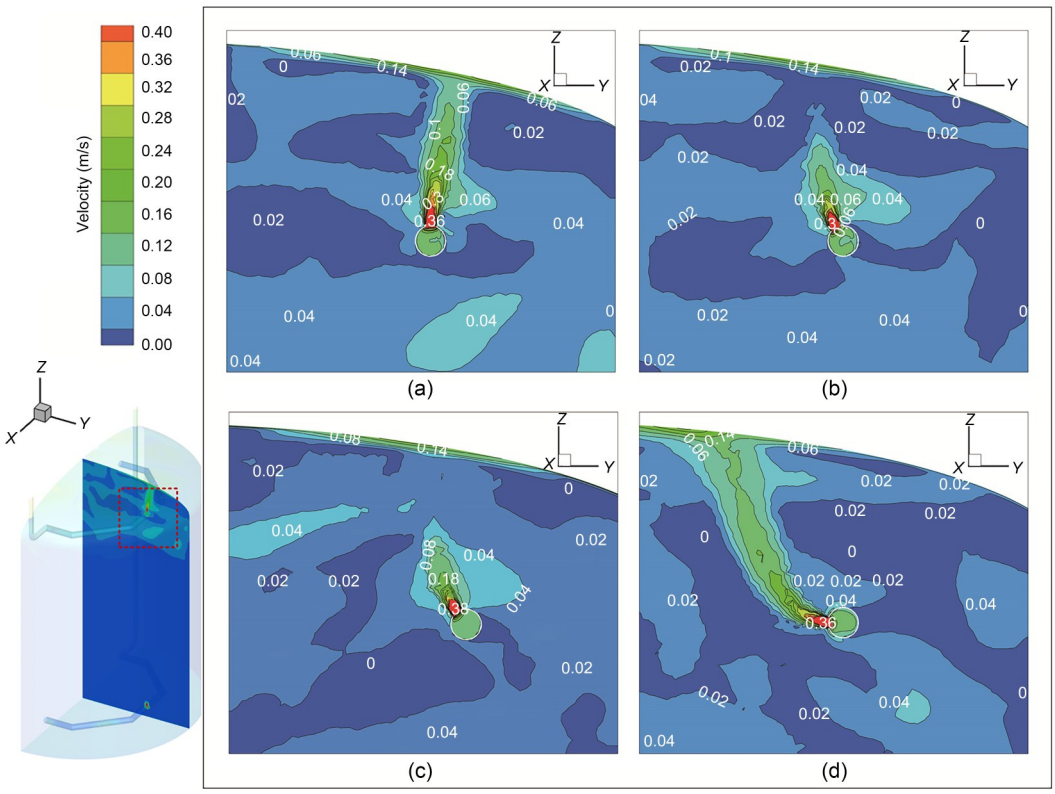

Fig. 18 Velocity contours of the impact jet in plane *X*=0 under different orifice angles: (a) 90°; (b) 60°; (c) 45°; (d) 0°

due to buoyancy and inertial forces. The impact jet strikes the vault wall at a relatively high velocity and over a longer distance, leading to enhanced mixing and a noticeable temperature change. When the orifice angle becomes oblique, specifically at 60° and 45°, the horizontal velocity component can improve heat exchange in the horizontal plane while reducing disturbance in the vertical direction. When the opening direction of orifices is horizontal, the buoyancy force surpasses the inertia force, causing the hot fluid to rise under the influence of buoyancy. This leads to a strong mixing effect between the hot and cold fluids, which could potentially hinder thermal delamination.

The thermocline performance was determined by the dimensionless thermocline volume V_{TK}^{*} (Fig. 19). Isosurfaces of 586 and 740 K were taken as isosurfaces with V_{TK}^{*} derived from the integration of the volume. The relationship between the opening angle and thermocline exhibited a non-monotonic trend, initially decreasing and subsequently thickening as the angle decreased. Notably, the thermocline thickness diminished with extended charging time. Consequently, in the design of storage tanks, neither vertical nor horizontal incidence should be favored; instead, an oblique incidence is preferable. The variations in V_{TK}^{*} between the opening directions of 60° and 45° at 3 and 4 h were negligible, amounting to less than 0.02%.

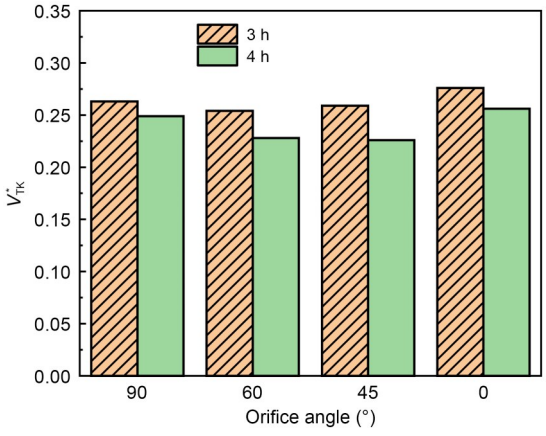

Fig. 19 Dimensionless volume of thermocline with different orifice angles

Through a comprehensive analysis, it is evident that the direction of the opening orifice significantly affects the angle and strength of the impact jet as hot fluid enters the TEST. This, in turn, influences the thickness of the thermocline. The inclined jet injection method can enhance the thermal stratification effect in molten salt storage tanks.

3.4 Comparison of the thermocline under different tube diameters

Three AADs with variable diameters, as supplied by the manufacturer, were subjected to simulation. All diffusers had a 45° orifice angle and ensured consistent inlet flow. The temperature fluctuation from 1 to 4 h along the central axis of the TEST was observed (Fig. 20). Between 1 and 2 h, at identical heights, the AAD with the smallest diameter exhibited the highest temperature, suggesting more vigorous mixing of cold and hot fluids. This phenomenon can be attributed to the fact that with equivalent flow rates, smaller tube diameters result in a higher flow speed within the tube, leading to a more pronounced turbulent effect from the outflow impact jet.

In the pursuit of managing production costs, selecting an AAD with a large diameter will yield superior thermal delamination outcomes.

3.5 Orifice diameter optimization

According to the analysis and comparison above, an AAD with a large tube diameter and oblique opening orifice provides superior thermal delaminating performance. However, the diffuser tube flow was not uniform, indicating room for further optimization of flow uniformity through adjustments in orifice size. Consequently, the orifice size in Case 7 was optimized using the method outlined in Section 2.3. The dimensionless volume of the thermocline after each iteration of optimization is illustrated in Fig. 21, and the optimized aperture distribution is shown in Table 5. The final thermocline thickness was reduced by 6.78% compared to the initial structure.

The temperature change curves for the five planes (denoted as P1 to P5, corresponding to Z=2, 4, 6, 8, and 10 m, respectively) in Cases 2 and 8 were monitored (Fig. 22). The subscripts “in” and “opt” represent the initial configuration and the optimized configuration, respectively. Prior to optimization, the rate of temperature change was slow, with notable heat loss occurring during the heat storage process of the P5 plane. This heat loss could be attributed to the mixing of cold and hot fluids, which makes it challenging to reach the desired working temperature of the fluid in the top layer. However, the optimized structure

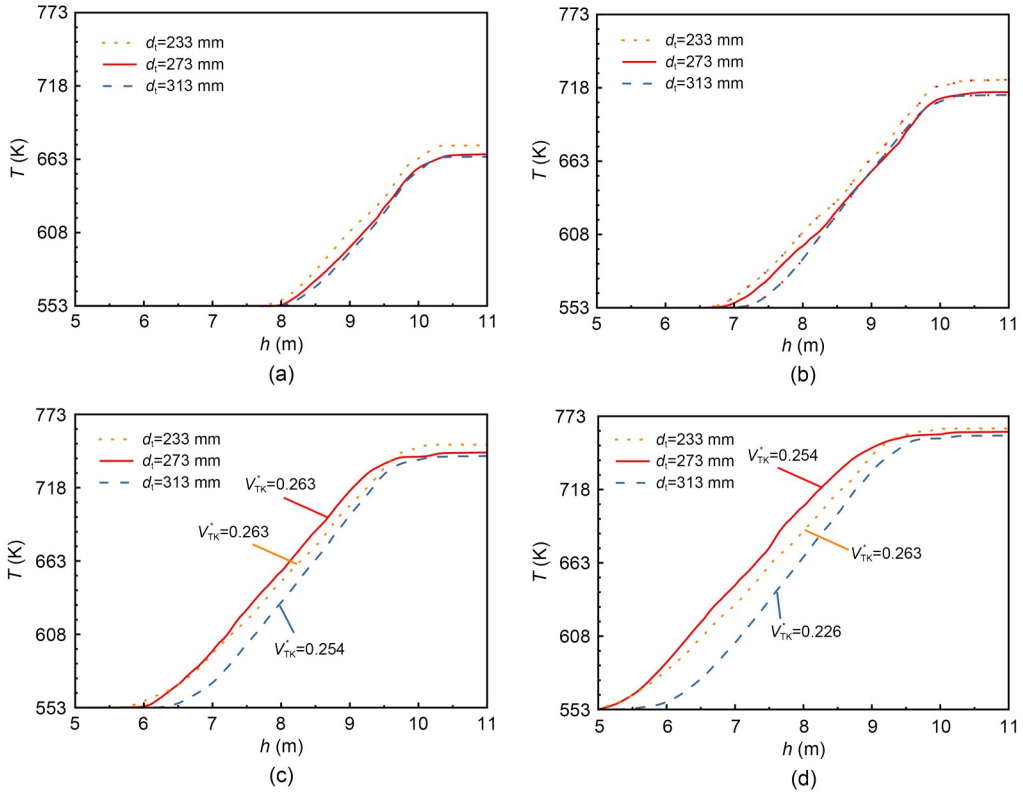

Fig. 20 Temperature curves in the TEST with different tube diameters: (a) t=1 h; (b) t=2 h; (c) t=3 h; (d) t=4 h

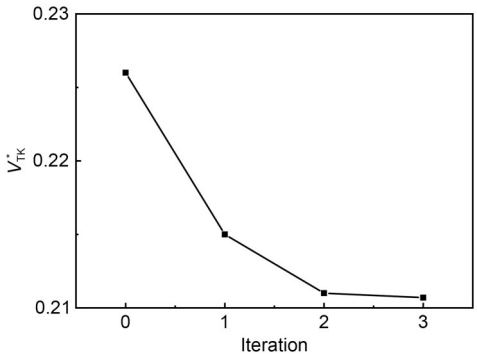

Fig. 21 Dimensionless thermocline volume V^*_{TK} after each iteration

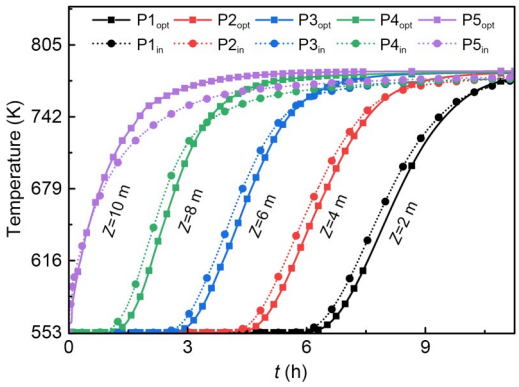

Fig. 22 Temperature change curves for different planes in Cases 2 and 8

Table 5 Orifice diameter

No.	Orifice diameter (mm)	
	Initial	Optimized
1	89	83.69
2	89	90.15
3	89	89.91
4	89	89.65
5	89	89.14
6	89	89.65
7	89	89.91
8	89	90.15

demonstrated a significant improvement in thermal stratification.

4 Conclusions

The thickness of the thermocline is a crucial factor influencing the efficacy of thermocline energy storage tanks (TESTs). This study used 3D transient computational fluid dynamics (CFD) simulations to

examine the evolution of the thermocline in TEST systems equipped with either an annular-arranged diffuser (AAD) or a cross-arranged diffuser (CAD), under realistic conditions. The accuracy of the model was confirmed through experimental data. The velocity attributes of the hot impact jet flow during the charging process were also scrutinized. A comparative analysis was conducted on the fluid mixing-dominated phases of the charging and discharging processes under both diffuser arrangements, using the trend variations in thermocline thickness as a reference. Notably, the uniformity of temperature across the diffuser plane was evaluated, along alterations in turbulent kinetic energy within the flow mixing zone. Additionally, the effects of the orifice opening angle and tube diameter on thermal delamination were explored. Based on these findings, a method for optimizing the orifice diameter to enhance temperature delamination characteristics was suggested. The results of our analysis were as follows:

1. In the actual scenario, due to the turbulent disturbance caused by the diffuser, the fluid did not maintain laminar flow in the mixed dominant region. Additionally, the flow characteristics in the circumferential direction lacked periodic symmetry due to the spatial arrangement of the diffusers.

2. The presence of a vaulted top resulted in a larger mixing region during the charging process than during the discharging process. Consequently, the formation time of a complete thermocline was extended.

3. The thermocline of the AAD was 4.23% and 5.41% thinner than that of the CAD during the charging and discharging processes, respectively. Therefore, AAD may be preferred in engineering applications.

4. The impact jet significantly influenced the thermocline thickness. In the TEST, an impact jet perpendicular to the temperature gradient enhanced axial flow mixing and reduced circumferential temperature diffusion, thereby increasing thermocline thickness. A diffuser orifice with an inclined angle is preferable.

5. The diameter of the diffuser's tube influenced temperature stratification characteristics. Considering the cost, it is advisable to opt for a diffuser with a large tube diameter.

6. The uniformity of temperature distribution within the TEST was enhanced by modifying the dimensions of the opening orifice in the diffuser. The proposed optimization method has the potential to decrease the thermocline by 6.78%.

In the context of future research, a design reference for diffusers of arbitrary shape was introduced via the collaborative optimization of stress distribution in both the diffuser and the tank. This approach enabled a comprehensive analysis of mechanical properties, extending beyond the fluid flow and heat transfer characteristics assessed in the TEST. Such an analysis is critical for the engineering design of diffusers and tanks. Investigating the manufacturing process of the designed diffuser within the TEST is another objective for subsequent studies.

Acknowledgments

This work is supported by the National Natural Science Foundation of China (No. 52375274), the Zhejiang Provincial Natural Science Foundation of China (No. LD21E050003), the Key R&D Program of Zhejiang Province (No. 2023C01229), and the Central Government Fund for Regional Science and Technology Development of China (No. 2023ZY1033).

Author contributions

Zheming TONG and Haidan WANG designed the research. Haidan WANG and Qi YANG processed the data. Haidan WANG wrote the first draft of the manuscript. Zheming TONG helped to organize the manuscript. Taotao NIE provided the original tank model. Zheming TONG, Haidan WANG, Shuiguang TONG, and Qi YANG revised and edited the final version.

Conflict of interest

Zheming TONG, Haidan WANG, Shuiguang TONG, Qi YANG, and Taotao NIE declare that they have no conflict of interest.

References

Afrin S, Kumar V, Bharathan D, et al., 2014. Computational analysis of a pipe flow distributor for a thermocline based thermal energy storage system. *Journal of Solar Energy Engineering*, 136(2):021010. https://doi.org/10.1115/1.4024927

Angelini G, Lucchini A, Manzolini G, 2014. Comparison of thermocline molten salt storage performances to commercial two-tank configuration. *Energy Procedia*, 49:694-704. https://doi.org/10.1016/j.egypro.2014.03.075

Cagnoli M, Gaggioli W, Liberatore R, et al., 2023. CFD modelling of an indirect thermocline energy storage prototype for CSP applications. *Solar Energy*, 259:86-98. https://doi.org/10.1016/j.solener.2023.05.019

Cascetta M, Cau G, Puddu P, et al., 2016. A comparison between CFD simulation and experimental investigation of a packed-bed thermal energy storage system. *Applied Thermal Engineering*, 98:1263-1272. https://doi.org/10.1016/j.applthermaleng.2016.01.019

Chandra YP, Matuska T, 2020. Numerical prediction of the

stratification performance in domestic hot water storage tanks. *Renewable Energy*, 154:1165-1179. https://doi.org/10.1016/j.renene.2020.03.090

Che S, Kim J, Jeon J, et al., 2024. Thermodynamic analysis of molten salt-based single-tank thermal energy storage system with heat transfer enhanced by gas injection. *Journal of Energy Storage*, 77:109959. https://doi.org/10.1016/j.est.2023.109959

Cheralathan M, Velraj R, Renganarayanan S, 2006. Heat transfer and parametric studies of an encapsulated phase change material based cool thermal energy storage system. *Journal of Zhejiang University-SCIENCE A*, 7(11):1886-1895. https://doi.org/10.1631/jzus.2006.A1886

Deng YJ, Sun DL, Niu MY, et al., 2021. Performance assessment of a novel diffuser for stratified thermal energy storage tanks–the nonequal-diameter radial diffuser. *Journal of Energy Storage*, 35:102276. https://doi.org/10.1016/j.est.2021.102276

ELSihy ES, Wang XH, Xu C, et al., 2021. Numerical investigation on simultaneous charging and discharging process of molten-salt packed-bed thermocline storage tank employing in CSP plants. *Renewable Energy*, 172:1417-1432. https://doi.org/10.1016/j.renene.2020.11.139

Gajbhiye P, Kedare S, Bose M, 2022. Experimental analysis of parameters influencing thermal stratification in single media single tank storage system with flow distributor. *Thermal Science and Engineering Progress*, 30:101243. https://doi.org/10.1016/j.tsep.2022.101243

Hosseinnia SM, Akbari H, Sorin M, 2021. Numerical analysis of thermocline evolution during charging phase in a stratified thermal energy storage tank. *Journal of Energy Storage*, 40:102682. https://doi.org/10.1016/j.est.2021.102682

Hua WS, Yan HF, Zhang XL, et al., 2022. Review of salt hydrates-based thermochemical adsorption thermal storage technologies. *Journal of Energy Storage*, 56:106158. https://doi.org/10.1016/j.est.2022.106158

Huang YH, Chen Q, 2016. Numerical investigation on thermal effects by adding thin compartmental plates into cooling enclosures with heat-leaking walls. *Journal of Zhejiang University-SCIENCE A (Applied Physics & Engineering)*, 17(6):485-496. https://doi.org/10.1631/jzus.A1500319

Joshi V, Wasnik C, Wadegaonkar A, et al., 2021. Influence of porosity and permeability of flow distributor on thermal stratification in single media storage tank. *Journal of Energy Storage*, 44:103241. https://doi.org/10.1016/j.est.2021.103241

Kaloudis E, Grigoriadis DGE, Papanicolaou E, 2016. Numerical simulations of constant-influx gravity currents in confined spaces: application to thermal storage tanks. *International Journal of Thermal Sciences*, 108:1-16. https://doi.org/10.1016/j.ijthermalsci.2016.04.018

Keilany MA, Milhé M, Bézian JJ, et al., 2020. Experimental evaluation of vitrified waste as solid fillers used in thermocline thermal energy storage with parametric analysis. *Journal of Energy Storage*, 29:101285. https://doi.org/10.1016/j.est.2020.101285

Khurana H, Majumdar R, Saha SK, 2024. Improved realistic stratification model for estimating thermocline thickness in vertical thermal energy storage undergoing simultaneous charging and discharging. *Journal of Energy Storage*, 82:110490. https://doi.org/10.1016/j.est.2024.110490

Kosman W, Rusin A, Reichel P, 2023. Application of an energy storage system with molten salt to a steam turbine cycle to decrease the minimal acceptable load. *Energy*, 266:126480. https://doi.org/10.1016/j.energy.2022.126480

Li SH, Zhang YX, Li Y, et al., 2014. Experimental study of inlet structure on the discharging performance of a solar water storage tank. *Energy and Buildings*, 70:490-496. https://doi.org/10.1016/j.enbuild.2013.11.086

Lou WR, Fan YL, Luo LG, 2020. Single-tank thermal energy storage systems for concentrated solar power: flow distribution optimization for thermocline evolution management. *Journal of Energy Storage*, 32:101749. https://doi.org/10.1016/j.est.2020.101749

Lou WR, Luo LG, Hua YC, et al., 2021. A review on the performance indicators and influencing factors for the thermocline thermal energy storage systems. *Energies*, 14(24):8384. https://doi.org/10.3390/en14248384

Lou WR, Baudin N, Roux S, et al., 2023a. Impact of buoyant jet entrainment on the thermocline behavior in a single-medium thermal energy storage tank. *Journal of Energy Storage*, 71:108017. https://doi.org/10.1016/j.est.2023.108017

Lou WR, Xie BS, Aubril J, et al., 2023b. Optimized flow distributor for stabilized thermal stratification in a single-medium thermocline storage tank: a numerical and experimental study. *Energy*, 263:125709. https://doi.org/10.1016/j.energy.2022.125709

Mahmoudinezhad S, Sadi M, Ghiasirad H, et al., 2023. A comprehensive review on the current technologies and recent developments in high-temperature heat exchangers. *Renewable and Sustainable Energy Reviews*, 183:113467. https://doi.org/10.1016/j.rser.2023.113467

Manu KV, Anand P, Chetia UK, et al., 2015. Effects of instabilities and coherent structures on the performance of a thermocline based thermal energy storage. *Applied Thermal Engineering*, 87:768-778. https://doi.org/10.1016/j.applthermaleng.2015.05.072

Nallusamy N, Sampath S, Velraj R, 2006. Study on performance of a packed bed latent heat thermal energy storage unit integrated with solar water heating system. *Journal of Zhejiang University-SCIENCE A*, 7(8):1422-1430. https://doi.org/10.1631/jzus.2006.A1422

Pacheco JE, Showalter SK, Kolb WJ, 2002. Development of a molten-salt thermocline thermal storage system for parabolic trough plants. *Journal of Solar Energy Engineering*, 124(2):153-159. https://doi.org/10.1115/1.1464123

Parida DR, Advaith S, Dani N, et al., 2022. Assessing the impact of a novel hemispherical diffuser on a single-tank sensible thermal energy storage system. *Renewable Energy*, 183:202-218.

https://doi.org/10.1016/j.renene.2021.10.099

Pizzolato A, Donato F, Verda V, et al., 2015. CFD-based reduced model for the simulation of thermocline thermal energy storage systems. *Applied Thermal Engineering*, 76:391-399. https://doi.org/10.1016/j.applthermaleng.2014.11.029

Prieto C, Tagle-Salazar PD, Patiño D, et al., 2024. Use of molten salts tanks for seasonal thermal energy storage for high penetration of renewable energies in the grid. *Journal of Energy Storage*, 86:111203. https://doi.org/10.1016/j.est.2024.111203

Shi H, Zhou H, Ma PN, et al., 2021. Experimental investigation of migration and solidification of molten salt leaking through tank cracks. *Journal of Zhejiang University-SCIENCE A (Applied Physics & Engineering)*, 22(12):979-991. https://doi.org/10.1631/jzus.A2100011

Tong ZM, Chen X, Tong SG, et al., 2022. Dense residual LSTM-attention network for boiler steam temperature prediction with uncertainty analysis. *ACS Omega*, 7(13): 11422-11429. https://doi.org/10.1021/acsomega.2c00615

Tong ZM, Wang HD, Tong SG, et al., 2023. Investigating the thermal-hydraulic enhancement and ash deposition characteristics of leeward-cut spiral finned tube heat exchangers. *International Communications in Heat and Mass Transfer*, 149:107145. https://doi.org/10.1016/j.icheatmasstransfer.2023.107145

Votyakov EV, Bonanos AM, 2015. Algebraic model for thermocline thermal storage tank with filler material. *Solar Energy*, 122:1154-1157. https://doi.org/10.1016/j.solener.2015.10.047

Weiss J, Ortega-Fernández I, Müller R, et al., 2021. Improved thermocline initialization through optimized inlet design for single-tank thermal energy storage systems. *Journal of Energy Storage*, 42:103088. https://doi.org/10.1016/j.est.2021.103088

Xu C, Liu M, Tang HY, et al., 2023. Thermodynamic analysis of the thermocline storage tank with time-varying charging parameters. *Applied Thermal Engineering*, 219:119477. https://doi.org/10.1016/j.applthermaleng.2022.119477

Yin HB, Ding J, Jiang RH, et al., 2017. Thermocline characteristics of molten-salt thermal energy storage in porous packed-bed tank. *Applied Thermal Engineering*, 110:855-863. https://doi.org/10.1016/j.applthermaleng.2016.08.214

Zhang QJ, Dong JN, Chen H, et al., 2024. Dynamic characteristics and economic analysis of a coal-fired power plant integrated with molten salt thermal energy storage for improving peaking capacity. *Energy*, 290:130132. https://doi.org/10.1016/j.energy.2023.130132